# Indirect polarization alignment with points on the sky, the Hub Test

*Richard Shurtleff* *

November 3, 2020

**Abstract**

The alignment of transverse vectors on the sky, such as the polarization directions of electromagnetic radiation from astronomical sources, can be an interesting property of the sources themselves or of the intervening medium between source and detector. Position angle tests directly compare two such vectors located at different points on the sky. The "Hub test" introduced here is indirect, based on the 'alignment' of the polarization direction at a source and other points on the sky. Simple formulas, easily applied, determine the significance of Hub test results. In some cases, the Hub test and the position angle tests agree, but in others the Hub test can find correlations even when position angles differ greatly. The Hub test is applied to a catalog of QSO polarization directions as an illustration.

Keywords: Polarization ; Alignment ; Large scale structure

## 1 Introduction

Large scale alignments are found for both optical and radio quasi stellar objects (QSOs). [1–3] In these studies, the tests that determine significant alignment compare the linear polarization directions of the electromagnetic radiation from the QSOs. An example of the potential value of such research is the finding of correlations between polarization directions and the local large scale structure. [4, 5]

The 'S' and 'Z' tests used to find alignments in Ref. [1–3] compare polarization position angles, PPAs, directly, which means that the polarization directions are significantly aligned when the PPAs clump together at some common value. When the objects in the sample are far apart, the curvature of the Celestial Sphere, usually hereafter called the 'sphere,' complicates the analysis because one must enlist a parallel translation rule to decide what directions are parallel. The complications have been faced and resolved. 'S' and 'Z' tests are well documented and reliably detect this type of alignment.

In this paper we pursue an alternative geometrical concept: the alignment of a direction with a point on the sky. The concept is evident to those in the Northern hemisphere who have observed that the direction at the star Merak toward Dubhe is aligned with the direction toward Polaris, a bit off, but close. For multiple sources, with many polarization directions at scattered locations, consider an analogy with the velocity vectors of passenger jets that are aligned because the jets are inbound to the same hub airport. That picture gives the Hub test its name.

Radial alignment is a case that would be detected by the Hub test and not by tests that compare polarization vectors directly. With all polarizations directed toward a common central point near the sources,

*affiliation and mailing address: Department of Sciences, Wentworth Institute of Technology, 550 Huntington Avenue, Boston, MA, USA, 02115, telephone number: (617) 989-4338, fax number: (617) 989-4591 , orcid.org/0000-0001-5920-759X, e-mail addresses: shurtleffr@wit.edu, momentummatrix@yahoo.com

the PPAs are very different and definitely not parallel, but yet they are in a certain sense aligned. They are aligned radially.

Suppose a linear filamentary electric current is directed along the sight of an observer, seen end-on. Then, by Ampere's Law, magnetic fields wrap around the current. These fields may act to orient molecules. Any EM radiation observed near the filament could develop a polarization or have its polarization component changed by interaction with the molecules. The radiation would then be polarized radially toward a central point near the location of the filament on the sky. Such a scenario could produce an effect that is detectible by the Hub test, but not by tests that directly compare linear polarization directions.

In general, astronomical sources are candidates for an alignment test if there is an observed asymmetry such as linear polarization or some other feature like a jet or an axis of rotation. The alignment of linear polarization directions is discussed here, but the test is easily adapted to other features. Also, the notion of 'avoidance' is measurable. Do the polarization directions avoid a point on the sphere? Avoidance is just as easy to measure with the Hub test as it is to measure alignment.

The Hub test requires seven or more sources complete with positions and polarization directions. Geometrically, two points in the sky determine a great circle, so the mathematical requirement is three sources, but the significance formula is an approximation that is not sufficiently accurate for three sources. We put the cutoff at seven sources. The process and needed formulas are presented in Sec. 2 and Sec. 3 discusses statistics, uncertainties and formulas for evaluating significance.

In Sec. 4, the Hub test is applied to a subset of the JVAS/CLASS 8.4GHz [6] catalog of partially polarized radio sources that were later identified as QSOs. [7]. The Hub test shown to be central to connecting a large, extended region of sources with very significantly aligned polarization directions. Perhaps due to their concepts of alignment, the S and Z tests found parts, but not the whole region to have aligned polarization directions.

Four QSO samples are discussed that are found by the Hub test to be very significantly aligned. Agreement with the S and Z tests is found in two regions coincident with regions previously discussed in Ref. [7]. Between these two regions, the sources in a third region are found to be significantly aligned only by the Hub test. The fourth sample combines the previous three into an extended region whose sources are very significantly aligned. The Hub test is central to the discovery of that large extended region of sources with aligned polarization directions. The Hub test introduces a new concept of alignment that may be combined with the other tests to help find any correlations of observed transverse polarization vectors.

## 2 The Hub Test

The data required to run the Hub test consists of 'sources' and a 'polarization direction' at each source. For convenience it is assumed that the position of each source on the Celestial sphere is given in equatorial coordinates. In this report, we use Right Ascension and Declination, $(\alpha, \delta)$, sometimes in degrees and sometimes in radians, to locate the sources on the sphere. The polarization directions are assumed to be position angles $\psi$ measured clockwise from the local North with East to the right. Since East is to the right, the point of view is outside the sphere looking down toward the Earth or Solar System.

As shown in Fig. 1(a), the "alignment angle" $\eta$, of a transverse polarization direction at a source $S$ with a point $H$ in the sky can be defined as the angle $\eta$ between two great circles, one with the polarization direction as its tangent and the other connecting $S$ and $H$. In (b) one sees that the alignment angle is the angle $\eta$ at the source between the tangents to the two great circles.

The angle $\eta$ is the same for all points on the great circle connecting $S$ and $H$. But the only point that is on all great circles through $H$ is the diametrically opposite point $-H$. So when there are many sources

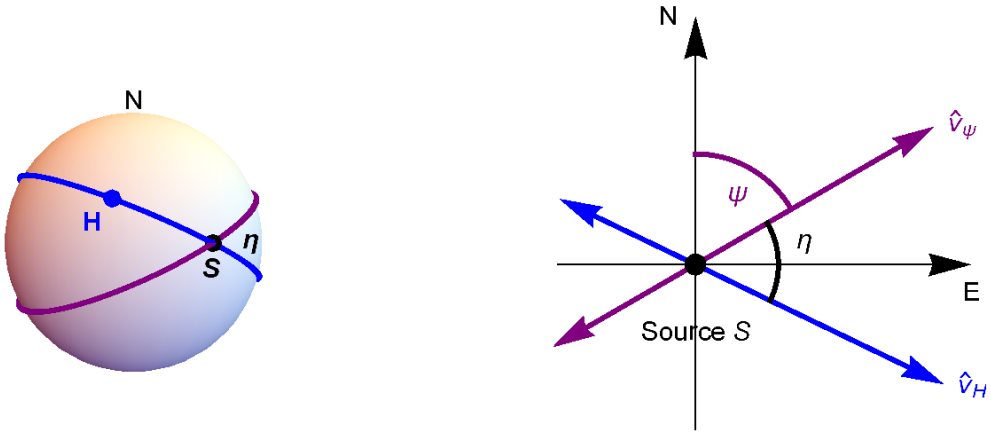


Figure 1: (Color online) *A source $S$ of polarized EM radiation and a point $H$ are plotted on the Celestial sphere.* (a) The source $S$ and point $H$ determine a great circle. The polarization direction is tangent to a second great circle. The angle $\eta$ is the acute angle between the two circles at $S$. (b) In the plane tangent to the Celestial sphere at $S$, the polarization position angle PPA is an angle $\psi$ measured clockwise from North with East to the right. The angle $\eta$ quantifies how well the polarization direction $\hat{v}_\psi$ aligns with the direction $\hat{v}_H$ toward $H$ from $S$.

with many angles $\eta$, the value of each $\eta$ is the same for $H$ and $-H$; the angle $\eta$ is a diametrically symmetric function of the point $H$.

Also note that the the angle $\eta$ is not uniquely defined when either $H$ or $-H$ coincides with the source $S$. Then no unique great circle connects $S$ with $H$, one can think that all great circles through the source $S$ fit the definition. However interpreted, one cannot define $\eta$ when $S$ or $-S$ coincides with $H$ or $-H$.

For the source $S$ in Fig. 1, let its location on the sphere be (RA,dec) = $(\alpha_S, \delta_S)$. Then the unit 3-vector $\hat{\mathbf{r}}_S$ from the center of the sphere at the origin $\{0,0,0\}$ to the source $S$ has Cartesian coordinates found by applying the general formula for any $(\alpha, \delta)$,

$$\hat{\mathbf{r}} = (x, y, z) = (\cos\alpha\cos\delta,\ \sin\alpha\cos\delta,\ \sin\delta)\ . \tag{1}$$

We write the radial vector formula converting (RA,dec) to Cartesian coordinates as a general formula because it will be needed in other contexts.

The Cartesian coordinates of unit vectors, $\hat{\mathbf{v}}_\mathrm{N}$ and $\hat{\mathbf{v}}_\mathrm{E}$, in the direction of local North and local East in the plane tangent to the sphere at $S$ are given by

$$\hat{\mathbf{v}}_\mathrm{N} = (-\cos\alpha\sin\delta,\ -\sin\alpha\sin\delta,\ \cos\delta)\ ;\ \hat{\mathbf{v}}_\mathrm{E} = (-\sin\alpha,\ \cos\alpha, 0)\ . \tag{2}$$

The three vectors $\hat{\mathbf{r}}_S$, $\hat{\mathbf{v}}_\mathrm{N}$, and $\hat{\mathbf{v}}_\mathrm{E}$ form an orthonormal set.

In the tangent plane at $S$, from Fig. 1(b), it is clear that the unit vector $\hat{\mathbf{v}}_\psi$ that points in the direction of the polarization position angle PPA $\psi$ is a linear combination of $\hat{\mathbf{v}}_\mathrm{N}$ and $\hat{\mathbf{v}}_\mathrm{E}$. We have

$$\hat{\mathbf{v}}_\psi = \cos\psi\,\hat{\mathbf{v}}_\mathrm{N} + \sin\psi\,\hat{\mathbf{v}}_\mathrm{E} \quad ; \quad \hat{\mathbf{n}}_{S\times\psi} = \hat{\mathbf{r}}_S \times \hat{\mathbf{v}}_\psi = \sin\psi\,\hat{\mathbf{v}}_\mathrm{N} - \cos\psi\,\hat{\mathbf{v}}_\mathrm{E}\,, \tag{3}$$

where the unit vector $\hat{\mathbf{n}}_{S\times\psi}$ is a cross product. As a cross product, it is perpendicular to both $\hat{\mathbf{r}}_S$ and to $\hat{\mathbf{v}}_\psi$. Since $\hat{\mathbf{n}}_{S\times\psi}$ is perpendicular to $\hat{\mathbf{r}}_S$, it lies in the plane tangent to the sphere at $S$ and is perpendicular to $\hat{\mathbf{v}}_\psi$. To avoid overcrowding, $\hat{\mathbf{n}}_{S\times\psi}$ is not drawn in Fig. 1(b). One can show that the three vectors $\hat{\mathbf{r}}_S$, $\hat{\mathbf{v}}_\psi$, $\hat{\mathbf{n}}_{S\times\psi}$ form an orthonormal set.

Let the point $H$ on the sphere in Fig. 1 be located at (RA,dec) $= (\alpha_H, \delta_H)$. The point $H$ must not be at the source $S$ or its diametrically opposite point $-S$. By avoiding $S$ and $-S$, there is a unique great circle that contains both $H$ and $S$. Clearly, the great circle lies in the plane spanned by $\hat{\mathbf{r}}_H$ and $\hat{\mathbf{r}}_S$.

The unit vector $\hat{\mathbf{v}}_H$ tangent to the great circle at the source $S$ lies in the plane of the great circle and must, therefore, be a linear combination of $\hat{\mathbf{r}}_H$ and $\hat{\mathbf{r}}_S$.

Since $\hat{\mathbf{v}}_H$ is tangent to the sphere at $S$, we know that $\hat{\mathbf{v}}_H$ is perpendicular to $\hat{\mathbf{r}}_S$. By applying the Gram-Schmidt process to $\hat{\mathbf{r}}_H$ and $\hat{\mathbf{r}}_S$, we get $\hat{\mathbf{v}}_H$ from $\hat{\mathbf{r}}_H$ by subtracting off the part of $\hat{\mathbf{r}}_H$ that is parallel to $\hat{\mathbf{r}}_S$. The result is

$$\hat{\mathbf{v}}_H = \frac{\hat{\mathbf{r}}_H - (\hat{\mathbf{r}}_S \cdot \hat{\mathbf{r}}_H)\hat{\mathbf{r}}_S}{\mid \hat{\mathbf{r}}_H - (\hat{\mathbf{r}}_S \cdot \hat{\mathbf{r}}_H)\hat{\mathbf{r}}_S \mid}\,, \tag{4}$$

where the dot product $\hat{\mathbf{r}}_S \cdot \hat{\mathbf{r}}_H = \cos\theta$ is the cosine of the angle between unit vectors $\hat{\mathbf{r}}_H$ and $\hat{\mathbf{r}}_S$. Since the denominator is the length of the vector in the numerator, the result is a unit vector.

The fundamental quantity in the Hub test is the alignment angle $\eta$ between the polarization direction $\psi$ and the direction toward the point $H$, as illustrated in Fig. 1. One can determine $\eta$ from the dot product of unit vectors $\hat{\mathbf{v}}_H$ and $\hat{\mathbf{v}}_\psi$,

$$\cos\eta = \mid \hat{\mathbf{v}}_H \cdot \hat{\mathbf{v}}_\psi \mid\ . \tag{5}$$

The absolute value is meant to assure that the alignment angle $\eta$ is acute, $0° \le \eta \le 90°$. The angle $\eta$ can be chosen to be acute because the electric field polarization direction and the tangent to the great circle from $S$ to $H$ are not oriented: the electric field oscillates back and forth along $\pm\hat{\mathbf{v}}_\psi$ and both directions $\pm\hat{\mathbf{v}}_H$ connect $S$ to $H$.

Consider the unit vector $\hat{\mathbf{n}}_{S\times H}$ that is perpendicular to the plane of the great circle through $H$ and $S$,

$$\hat{\mathbf{n}}_{S\times H} = \frac{\hat{\mathbf{r}}_S \times \hat{\mathbf{r}}_H}{\mid \hat{\mathbf{r}}_S \times \hat{\mathbf{r}}_H \mid}\,. \tag{6}$$

By the properties of cross products, the unit vector $\hat{\mathbf{n}}_{S\times H}$ is perpendicular to both $\hat{\mathbf{r}}_S$ and $\hat{\mathbf{r}}_H$. Thus $\hat{\mathbf{n}}_{S\times H}$ is in the plane tangent to the sphere at $S$. By (4), $\hat{\mathbf{v}}_H$ is a linear combination of $\hat{\mathbf{r}}_S$ and $\hat{\mathbf{r}}_H$, it follows that $\hat{\mathbf{n}}_{S\times H}$ is perpendicular to $\hat{\mathbf{v}}_H$. Thus the vector $\hat{\mathbf{n}}_{S\times H}$ lies in the plane tangent to the sphere at $S$ in a direction perpendicular to $\hat{\mathbf{v}}_H$. To avoid overcrowding, the vector $\hat{\mathbf{n}}_{S\times H}$ is not drawn in Fig. 1(b).

In the plane tangent to the sphere at $S$, the perpendicular directions $\hat{\mathbf{n}}_{S\times H} \perp \hat{\mathbf{v}}_H$ and $\hat{\mathbf{n}}_{S\times\psi} \perp \hat{\mathbf{v}}_\psi$ differ by the same angle as $\hat{\mathbf{v}}_H$ and $\hat{\mathbf{v}}_\psi$. Thus, as an alternate to (5) one can also determine $\eta$ from

$$\cos\eta = \mid \hat{\mathbf{n}}_{S\times\psi} \cdot \hat{\mathbf{n}}_{S\times H} \mid\ . \tag{7}$$

Whether one uses (5) or (7), the formulas (1) through (7) allow the alignment angle $\eta$ to be calculated given the PPA $\psi$ and the locations $(\alpha_S, \delta_S)$ and $(\alpha_H, \delta_H)$ of the source $S$ and point $H$ on the sphere.

Suppose the Hub test is applied to a sample, a collection of many sources $S_i$, $i \in 1, ..., N$, where $N$ is the number of sources. Each source $S_i$ has a given location on the sphere, $(\alpha_i, \delta_i)$, that is part of the original data. Each source has a polarization direction determined by a polarization position angle PPA denoted $\psi_i$. Then, for each source $S_i$ and each point $H$ on the sphere, there is an alignment angle $\eta_{iH}$, as pictured in Fig. 1, but now for $N$ sources.

For almost all points $H$ on the sphere, one can define an average alignment angle function $\bar{\eta}(H)$ representing how well aligned with $H$, on average, are the polarization directions of the collection of sources $S_i$. Let the function $\bar{\eta}(H)$ be defined as

$$\bar{\eta}(H) = \bar{\eta}(\alpha, \delta) = \frac{1}{N} \sum_i \eta_{iH} \,, \tag{8}$$

where (RA,dec) = $(\alpha, \delta)$ is the location of $H$. To be more precise, this is the arithmetic mean. Plots of the function $\bar{\eta}(\alpha, \delta)$ are displayed in Figs. 4 and 5.

As commented after (5), all the alignment angles $\eta_{iH}$ are acute angles. It follows that their average, $\bar{\eta}(H)$, is an acute angle, $0° \leq \bar{\eta}(H) \leq 90°$.

The function $\bar{\eta}(H)$ cannot be defined where $H$ or $-H$ is coincident with any of the sources, $\pm H \neq S_i$. From Fig. 1, when $S$ and $H$ are the same point, infinitely many great circles 'connect' them, so there is no well defined angle $\eta$. In the formulas, $\hat{\mathbf{v}}_H$ in (4) is indeterminate, 0/0, when $\hat{\mathbf{r}}_H$ and $\hat{\mathbf{r}}_S$ coincide.

As noted earlier, the angle $\eta$ in Fig. 1 is a diametrically symmetric function of $H$, so the average of many $\eta$s, $\bar{\eta}(H)$, is also diametrically symmetric,

$$\bar{\eta}(H) = \bar{\eta}(-H) \,. \tag{9}$$

The maximum and minimum values of the $\bar{\eta}(H)$ have special meanings. The Hub test provides numerical results $\bar{\eta}_{\min}$ and $\bar{\eta}_{\max}$ that can be used to judge how strongly the sources' polarization directions are correlated with $H_{\min}$ and $H_{\max}$. The locations of the max and min points on the sphere, $H_{\min}$ and $H_{\max}$, that the polarization directions tend to point towards or away from are also potentially useful information determined by the test.

The maximum alignment angle $\bar{\eta}_{\max}$ occurs at some point $H_{\max}$ and is a measure of how well the polarization vectors together avoid the direction toward $H_{\max}$, which is, one might call the sample's "unhub". The points $H_{\max}$ and $-H_{\max}$ are the most unaligned points on the sphere. While such points may be of interest for some purposes, in this article we are more interested in how well the polarization directions align. The symmetry between avoidance and alignment should be noted.

For the Hub test, the alignment of the polarization directions for a given collection of sources is quantified by the minimum alignment angle $\bar{\eta}_{\min}$. With perfect alignment all polarization directions point to the same hub and that means $\bar{\eta}_{\min}$ would vanish. The smaller the angle, the better aligned the polarization directions. For this article, testing alignment is the central purpose. Other information is also made available, such as, but not limited to, the location of the hubs $\pm H_{\min}$, and the results for the maximum avoidance, $\bar{\eta}_{\max}$, and $\pm H_{\max}$.

Once one has determined the best alignment angle $\bar{\eta}_{\min}$ for the observed data, it is important to know how likely random polarization directions would have returned an equivalent or better result. The problem of significance is treated next.

# 3 Significance Level and Uncertainty

How do we know if the alignment is significant? What is the likelihood that sources with random PPA polarization angles would produce a lower $\bar{\eta}_{\min}$ or a higher $\bar{\eta}_{\max}$? To find out, we repeat the process in Sec. 2, making many runs with sources that have randomly polarized PPA data. The many results produce raw probability distributions that can be approximated with functions. These functions can be used to determine the significance of observed alignments.

One expects that the number of sources is an important parameter. Runs with a small number of sources are more likely to have lower $\bar{\eta}_{\min}$ and higher $\bar{\eta}_{\max}$ when compared to runs with large numbers of sources.

The random run process we use is keyed to the example in Sec. 4 below. The sources are located in regions with given radii $\rho$, $\rho \in \{180°, 24°, 12°, 5°, 0°\}$. By the diametrical symmetry of the alignment angles $\eta$, the 180° case covers sources anywhere on the whole sphere. And $\rho = 0°$ is point-like; all sources are confined to a very small region.

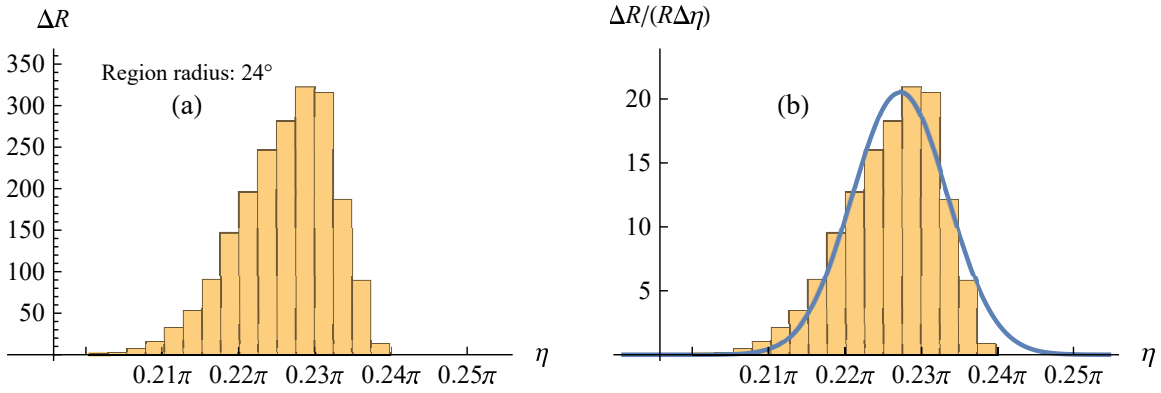


Figure 2: (Color online) $R = 2000$ *runs for* $N = 181$ *sources with random polarization PPA* $\psi$. For each run, the sources were assigned random polarization directions $\psi$. The best alignment angle $\bar{\eta}_{\min}$ for each of the $R$ runs was collected and the results analyzed. In (a), the histogram of the number of runs $\Delta R$ in each bin of width $\Delta\bar{\eta} = 0.0025\pi$ radians. The total number of runs is the sum of the bar heights, $R = \sum \Delta R$. Thus, by dividing by $R\Delta\bar{\eta}$, the sum of the areas of the bars in (b) is unity, an approximation to the probability distribution. The normal distribution, (10), that fits the data is plotted in the foreground.

The random runs use the same $2° \times 2°$ grid that is constructed for the example in Sec. 4. Since location is irrelevant for the random runs, the sources are confined to a single region for all runs, a region centered near the grid point at (RA,dec) = $(70.4°, 58.0°)$. Sources are chosen at random from the grid points within the region and moved slightly off-grid to avoid resonances. For point-like regions with null radii, $\rho = 0°$, the math was simpler with the sources at the North pole. The number of sources $N$ in a given run is taken from the set $\{4, 8, 16, 32, 64, 128, 181, 256, 512\}$, *i.e.* powers of 2 and 181. The number 181 is special because the central region discussed in Sec. 4 has 181 sources. Each source is assigned a PPA $\psi$ polarization angle chosen at random from 0° to 180°.

A random run starts by choosing $N$ sources at random locations in the region and assigning random PPA $\psi$ polarization angles to each. The alignment angle $\eta_{iH}$ between the $i$th source and the grid point $H$ is calculated as in Sec. 2. The average (arithmetic mean) $\bar{\eta}_H$ of the $N$ alignment angles $\eta_{iH}$ at each grid point $H$ is calculated. The largest and smallest average alignment angles, $\bar{\eta}_{\min}$ and $\bar{\eta}_{\max}$, are determined as well as the hub locations $H_{\min}$ and $H_{\max}$ where the extreme angles occur. The locations of the sources, their PPA angles $\psi$, the location $H_{\min}$, the smallest average alignment angle $\bar{\eta}_{\min}$, the location $H_{\max}$, and the largest average alignment angle $\bar{\eta}_{\max}$ are collected in a table and stored. That completes the random run.

Many random runs were completed for this article. The sources were confined to regions of radii $\{0°, 5°, 12°, 24°, 180°\}$. By diametrical symmetry, the 180° region effectively covers the entire sphere. The number $N$ of sources in each region were assigned to be $N = \{4, 8, 16, 32, 64, 128, 181, 256, 512\}$, *i.e.* powers of two plus $N = 181$. There were $R = 2000$ runs for the case of the 24° region with $N = \{4, 8, 16, 32, 64, 128, 181\}$

sources. All other cases were run $R = 1000$ times.

In symbols, for $R(N)$ runs with a given number of sources $N$, there are a total of $R(N)$ values of $\bar{\eta}_{\rm min}$ and $\bar{\eta}_{\rm max}$. By counting the number $\Delta R_i^{\rm min}$ of values of $\bar{\eta}_{\rm min}$ that are found in an interval $\Delta\eta$ centered on $\eta_i$, one obtains a histogram, the collection $\{\eta_i, \Delta R_i^{\rm min}\}$. Since the total number of runs is the sum, $R = \sum \Delta R_i$, the fraction of random results $\bar{\eta}_{\rm min}$ that are in the $i$th bin is $\Delta R_i/R$.

A histogram for random runs in a 24° radius region with $N = 181$ sources is plotted in Fig. 2(a). In part (b), the probability distribution is approximated by a normal distribution $P(\eta)$,

$$P(\eta) = \frac{1}{\sigma\sqrt{2\pi}} e^{-\frac{1}{2}\left(\frac{\eta-\eta_0}{\sigma}\right)^2} \quad , \tag{10}$$

where $2\sigma$ is the 'width', with $P(\eta_0 \pm \sigma) = e^{-1/2} P(\eta_0)$, and $\eta_0$ is the most likely value of $\eta$, the 'mean'. Both $\eta_0(N)$ and $\sigma(N)$ are functions of the number of sources $N$ in the sample. The likelihood that a random result $\bar{\eta}_{\rm min}$ is in an interval $\delta\eta$ centered on $\eta$ is approximated by $P(\eta)\delta\eta$.

By fitting probability distributions (10) to histograms for $R(N)$ random runs with $N$ sources in a region of radius $\rho$ and $N = \{4, 8, 16, 32, 64, 128, 181, 256, 512\}$, one finds a mean value $\eta_0(N)$ and a half-width $\sigma(N)$ for each $N$. It turns out that the various $\eta_0(N)$ and $\sigma(N)$ are well described by simple functions of $\sqrt{N}$,

$$\eta_0^{\rm min}(N) = \frac{\pi}{4} - \frac{c_1}{\left(\sqrt{N}\right)^{a_1}} \approx \frac{\pi}{4} - \frac{1}{\sqrt{N}} \quad ; \quad \sigma^{\rm min}(N) = \frac{c_2}{4\left(\sqrt{N}\right)^{a_2}} \approx \frac{1}{4\sqrt{N}} \tag{11}$$

$$\eta_0^{\rm max}(N) = \frac{\pi}{4} + \frac{c_1}{\left(\sqrt{N}\right)^{a_1}} \approx \frac{\pi}{4} + \frac{1}{\sqrt{N}} \quad ; \quad \sigma^{\rm max}(N) = \frac{c_2}{4\left(\sqrt{N}\right)^{a_2}} \approx \frac{1}{4\sqrt{N}} \quad ,$$

where the parameters $c_i$ and $a_i$ for $\eta_0^{\rm min}$ and $\eta_0^{\rm max}$ have values near unity, depending on the radius $\rho$ of the region. In Table 1, we see that the $a_i$ are close to unity for all radii $\rho$, while $c_1$ and, to a lesser extent, $c_2$ are near one when $\rho > 5$. The simpler expressions in (11) apply when the parameters $a_i$ and $c_i$ are equal to one.

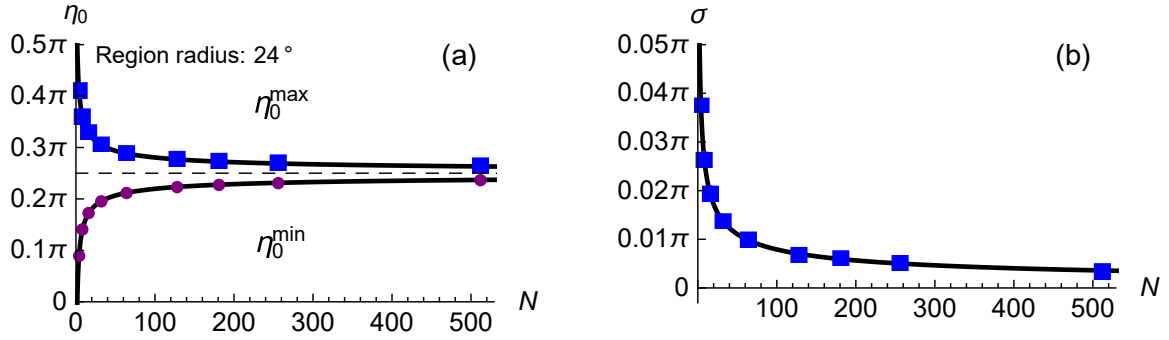


Figure 3: (Color online) *For $\rho = 24°$ radius regions, the mean $\eta_0$ and half-width $\sigma$ parameters for random runs as functions of the number of sources $N$ in (11) and Table 1.* (a) Note that avoidance (max) and alignment (min) are symmetric about the dashed line at the angle $0.25\pi = 45°$. (b) Since, for $\rho > 5°$, all of the parameters in Table 1 are roughly unity, $c_i, a_i \approx 1$, the half-widths $\sigma$ are about $1/(4\sqrt{N})$, which, by (11), is a quarter of the separation of the $\eta_0$ curves in (a) from the dashed centerline $\eta_0 = \pi/4$.

| Region Radius $\rho$ | $c_1^{\min}$ | $a_1^{\min}$ | $c_2^{\min}$ | $a_2^{\min}$ |
|---|---|---|---|---|
| 180° | $0.9992 \pm 0.0036$ | $1.0049 \pm 0.0031$ | $0.908 \pm 0.015$ | $0.985 \pm 0.014$ |
| 24° | $1.023 \pm 0.011$ | $1.0310 \pm 0.0098$ | $0.923 \pm 0.011$ | $0.9629 \pm 0.0099$ |
| 12° | $0.989 \pm 0.012$ | $1.033 \pm 0.011$ | $0.974 \pm 0.022$ | $0.993 \pm 0.019$ |
| 5° | $0.9082 \pm 0.0074$ | $1.0183 \pm 0.0071$ | $0.911 \pm 0.015$ | $0.944 \pm 0.014$ |
| 0° | $0.5526 \pm 0.0051$ | $1.0093 \pm 0.0080$ | $1.273 \pm 0.027$ | $1.072 \pm 0.019$ |
| Region Radius | $c_1^{\max}$ | $a_1^{\max}$ | $c_2^{\max}$ | $a_2^{\max}$ |
| 180° | $1.0224 \pm 0.0099$ | $1.0189 \pm 0.0085$ | $0.982 \pm 0.023$ | $1.037 \pm 0.021$ |
| 24° | $1.018 \pm 0.012$ | $1.026 \pm 0.010$ | $0.9172 \pm 0.0097$ | $0.9712 \pm 0.0090$ |
| 12° | $0.9982 \pm 0.0060$ | $1.0286 \pm 0.0053$ | $0.961 \pm 0.031$ | $0.986 \pm 0.027$ |
| 5° | $0.9089 \pm 0.0056$ | $1.0126 \pm 0.0054$ | $0.894 \pm 0.020$ | $0.942 \pm 0.019$ |
| 0° | $0.5482 \pm 0.0044$ | $1.0033 \pm 0.0070$ | $1.273 \pm 0.026$ | $1.072 \pm 0.018$ |

Table 1: *Parameters $c_i$ and $a_i$, $i$ = 1,2 in (11) for regions with various radii $\rho$.* By the symmetry across diameters, the region with a radius of 180° covers the whole sphere. The parameters $c_i$ for $\rho > 5°$ and $a_i$ for any $\rho$ are close to unity, some equal to one within the plus/minus standard error.

By the fundamental diametrical symmetry of great circles, we know that, if $H$ is a point on a great circle, then the diametrically opposed point $-H$ is also on the great circle. This implies that the region $\rho = 180°$ in Table 1 allows sources to be anywhere on the entire sphere, not just on a hemisphere.

One should not confuse the listings in Table 1 for a region with radius $\rho = 0°$ with results for an unpolarized source. An unpolarized or circularly polarized source has its linear polarization randomly or uniformly cycling though all directions perpendicular to the line of sight. Here we have $N$ definite and unchanging polarization directions from independent sources that happen to be located in a tiny region.

Note that, for random runs at $\rho = 5°$ and especially for $\rho = 0°$ with any given number $N$ of sources, the alignment and avoidance angles approach the midway value $\pi/4$ much closer than they do for larger regions. See Table 1, where $c_1$ is noticeably smaller for $\rho = 5°$ and 0° than it is for regions with larger radii $\rho$.

The dependence on $\sqrt{N}$ of $\eta_0^{\min}(N)$ and $\eta_0^{\max}(N)$ in (11) can be made plausible by adapting random walk ideas. [8] In random walk notation, at each point $H$ on the sphere, except at sources or opposite sources, define

$$D_N \equiv N\left(\bar{\eta}(H) - \frac{\pi}{4}\right) = \sum_i^N \left(\eta_{iH} - \frac{\pi}{4}\right) = D_{N-1} + s \quad , \tag{12}$$

where we use (8) and where $s$ is a 'step', the change that gives $D_N$ from $D_{N-1}$.

From Fig. 1, with a random polarization direction $\psi$ for the $N^{\text{th}}$ source, the alignment angle $\eta$ is as likely to be greater than $\pi/4$ as it is to be less than $\pi/4$. Thus the step $s = (\eta_{NH} - \pi/4)$ is as likely to be positive as it is to be negative. By repeating over many trials, we infer that the average step $s$ would vanish, $\langle s\rangle = 0$.

However, the square of $s$, *i.e.* $s^2$, is always positive or zero. Let us assume that the average of $s^2$ is a constant, $\langle s^2\rangle = d^2$, while maintaining $\langle s\rangle = 0$. Then the average of $D_N^2$ increases with $N$,

$$\langle D_N^2\rangle = \langle (D_{N-1} + s)^2\rangle = \langle D_{N-1}^2\rangle + \langle s^2\rangle = \langle D_1^2\rangle + (N-1)d^2 = Nd^2 \quad , \tag{13}$$

where we assume that $\langle D_1^2\rangle = d^2$. The root-mean-square value $D_N^{\text{rms}} \equiv \sqrt{\langle D_N^2\rangle} = \pm d\sqrt{N}$ and, by (12), we

have

$$\bar{\eta}^{\rm rms}(H) = \frac{\pi}{4} \pm \frac{d}{\sqrt{N}} \quad , \tag{14}$$

which is much like (11).

To make (14) equivalent to (11), the extreme value of the constant $d$ would need to be one radian. This means that the locations $H^{\rm min}$ and $H^{\rm max}$ of the extreme alignment angle, max or min, for $N-1$ sources are most likely near their locations for $N$ sources, while the added source contributes an amount $d^2$. To produce (11) from (14), one concludes that the added amount is one, $d^2 = \langle (\eta_{NH} - \pi/4)^2 \rangle = 1$, on average for max avoidance or best alignment. Justifying that conclusion is a more complicated problem than I want to consider here. So, let us settle for having shown that the dependence of $\eta_0^{\rm min}(N)$ and $\eta_0^{\rm max}(N)$ on $\sqrt{N}$ in (11) is made plausible by the coincidence of (11) and (14).

Fig. 3 plots the functions in (11) and the means $\eta_0(N)$ and the half-widths $\sigma(N)$ from random runs with sources in a $\rho = 24^\circ$ region.

Let us use Fig. 3 to visualize the probability distributions in (10) and (11). The bulk of the most likely alignment angles $\bar{\eta}_{\rm min}$ and avoidance angles $\bar{\eta}_{\rm max}$ extend vertically a little above and a little below the $\eta_0$ curves drawn in (a). The half-widths $\sigma$ in (b) are a quarter of the separation $1/\sqrt{N}$ in (a) between the angle $\pi/4$ to the $\eta_0$ curves, $\mid \pi/4 - \eta_0 \mid$ . So the max and min avoidance and alignment angles $\bar{\eta}$ of a given random run will most likely fall in two bands centered on the $\eta_0$ curves, bands whose half-widths $\sigma$ are about a quarter of the separation from $\pi/4$ to the $\eta_0$ curves. With that pictured, we leave random runs and return to observations.

Given an 'observed' alignment angle $\bar{\eta}_{\rm min}^{\rm obs}$, *i.e.* one that is calculated from observed polarizations, there is a chance that randomly directed polarizations can produce an equal or smaller alignment angle. The "significance" $S$ of a particular $\bar{\eta}_{\rm min}^{\rm obs}$ is defined to be the likelihood that random runs will show better alignment than indicated by the observed angle.

Similarly, there is a likelihood that the avoidance angle $\bar{\eta}_{\rm max}^{\rm obs}$, could be less than the result of some random run. We therefore define two significances $S^{\rm min}(\bar{\eta}_{\rm min}^{\rm obs})$ and $S^{\rm max}(\bar{\eta}_{\rm max}^{\rm obs})$, one for alignment and one for avoidance.

Given the Gaussian approximation $P_N(\eta)$ in (10) to the probability distribution, the significance of a minimum alignment angle $\bar{\eta}_{\rm min}^{\rm obs}$ is the integral from minus infinity to the observed angle,

$$S^{\rm min}(\bar{\eta}_{\rm min}^{\rm obs}) = \int_{-\infty}^{\bar{\eta}_{\rm min}^{\rm obs}} P_N(\eta) {\rm d}\eta \quad ; \quad S^{\rm max}(\bar{\eta}_{\rm max}^{\rm obs}) = \int_{\bar{\eta}_{\rm max}^{\rm obs}}^{\infty} P_N(\eta) {\rm d}\eta \quad . \tag{15}$$

The significance formula for an observed max avoidance angle $\bar{\eta}_{\rm max}^{\rm obs}$ in (15) follows by similar reasoning and indicates the likelihood that random runs would produce larger avoidance angles than the angle $\bar{\eta}_{\rm max}^{\rm obs}$ that is calculated from observed data.

Since the probability distributions are Gaussians, the integrals in (15) can be evaluated in terms of the error function, ${\rm erf}(z) \equiv \int_0^z \exp(-t^2) {\rm d}t$. Combining (10), (11), and (15), one finds that

$$S_N(\eta) = \frac{1}{2}\left(1 - {\rm erf}\left[2\sqrt{2} N^{\,a_2/2}\left(\frac{\mid \frac{\pi}{4} - \eta \mid - c_1 N^{\,-a_1/2}}{c_2}\right)\right]\right) \quad , \tag{16}$$

$$S_N(\eta) \approx \frac{1}{2}\left(1 - {\rm erf}\left[2\sqrt{2}\left(\mid \frac{\pi}{4} - \eta \mid \sqrt{N} - 1\right)\right]\right) \quad ,$$

where the simpler expression occurs for $c_i = a_i = 1$ and where the absolute value $\mid \frac{\pi}{4} - \bar{\eta} \mid$ allows writing both $S^{\rm min}$ and $S^{\rm max}$ in one expression. The further the average $\bar{\eta}(H)$ in (8) is below or above $\pi/4$, the more significant the alignment or avoidance of the polarization directions with the point $H$ on the sphere.

The normal distribution in (10) approximates the actual probability distribution of the results of random runs. Note that the distribution has nonzero values for any real $\eta$, positive or negative, while alignment and avoidance angles $\bar{\eta}$ are confined to a finite interval, *i.e.* they are nonnegative acute angles $0^\circ \leq \eta \leq 90^\circ$. So, there might be a problem.

Probabilities and significances are meaningless for PPA angles that are negative, $\bar{\eta} < 0^\circ$, or larger than a right angle, $\bar{\eta} > 90^\circ = \pi/2$ rad. With only slight differences due to the parameters $c_i$ and $a_i$, by (16), we have $S_N^{\min}(0) \approx S_N^{\max}(\pi/2)$, which means that the significance of the disallowed angles smaller than 0 and larger than $90^\circ = \pi/2$ are the same. For $N = 4$, one calculates $S_{N=4}^{\min}(0) \approx S_{N=4}^{\max}(\pi/2) = 0.007$, which is almost 1% and is not negligible when determining significance. But, by $N = 7$, one finds that $S_{N=7}^{\min}(0) \approx S_{N=7}^{\max}(\pi/2) = 2 \times 10^{-6}$ or two parts per million. That may be considered negligible. For the example discussed in the next section, only regions with seven or more sources are considered.

# 4 An application of the Hub test

In this section, the Hub test is applied to published data measured, collected and catalogued by others. The data is a subset of the the JVAS/CLASS 8.4-GHz catalog of more than 12700 radio sources. [6] After the catalog was published, a set of 1450 QSOs quasars (QSOs) in the catalog that meet certain requirements were identified. [7] A couple of the most relevant constraints are the limit on uncertainties in PPA, $\sigma_\psi \leq 14^\circ$, and the requirement that linear polarization percentages must exceed 0.6%. One motivation of the CLASS survey is to study Faraday rotations and so no corrections for Faraday rotation were applied to the data. See Refs. [6] and [7] for details and discussion.

In preparation for applying the Hub test, a $2^\circ \times 2^\circ$ grid was constructed on the celestial sphere, some 10,518 individual points. Each grid point serves as the center of a 24°-radius region. The QSO sources located in each region make one sample. With 2° spacing and 24° radii, neighboring regions overlap making changes gradual from one region to neighboring regions. The 2° spacing also means that any derived locations have uncertainties greater than half the smallest division, *i.e.* $(\Delta\text{RA}, \Delta\text{dec}) \geq (\pm 1^\circ/\cos\delta, \pm 1^\circ)$.

As discussed at the end of the previous section, the probability distribution and significance formulas are approximations that are not considered accurate enough for samples with fewer than seven sources. Thus, we consider here the 6801 regions that are populated with from 7 to 251 sources. The median population of these regions is 81 sources, with an arithmetic average of 95 sources. Applying the significance formula (16) yields 555 "very significantly" aligned regions. To be very significant, fewer than 1% of samples with randomly directed polarizations are better aligned.

While alignment is the focus of this article, one should note that there are 206 regions whose sources display significant avoidance, meaning fewer than 1% of random samples with the same number of sources would avoid some point on the sphere with a larger avoidance angle $\bar{\eta}_{\max}$. So, for these QSO sources, significant alignment is found more often, 555 versus 206, than significant avoidance.

The most significantly aligned region, whose sources are depicted as dots in Fig. 4(c), has 181 sources and a minimum alignment angle $\bar{\eta}_{\min} = 0.63$ rad $= 36.4^\circ$. Its significance is about one in one hundred thousand, $S_{181}(0.63) = 1.0 \times 10^{-5}$, meaning one in one hundred thousand 24° regions with 181 sources but with random polarization directions would be better aligned. The contour plot of $\bar{\eta}_{\min}$ for the region is displayed in part (c) of Fig. 4.

The sources in the regions in (a) and (b) of Fig. 4 are found by the Hub test to be very very significantly aligned. These regions approximate regions found to be very significantly aligned by the S and Z tests, see

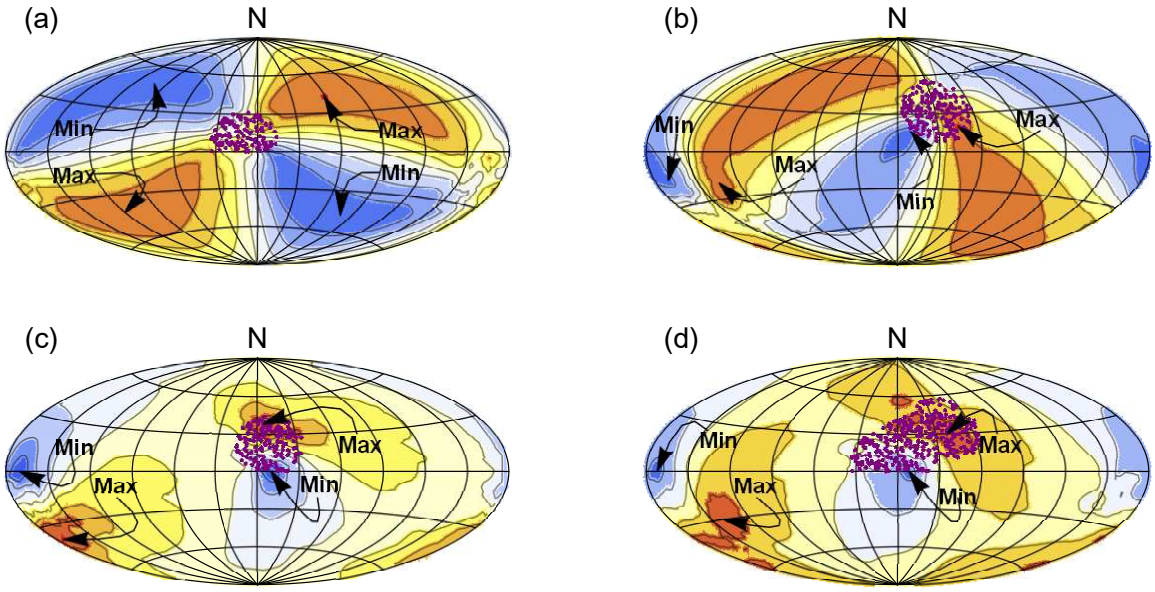


Figure 4: (Equatorial coordinates, Aitoff plots, 2° contours, Color online) *Alignment functions for various samples.* The sources are displayed as purple dots. At each point $H$ on the Celestial sphere, the angles $\eta$, as in Fig. 1, at the sources $S$ are averaged and that average $\bar{\eta}(H)$ becomes a function of location $H$ on the sphere. The function $\bar{\eta}(H)$ is plotted here for four regions of sources whose best alignment angle $\bar{\eta}_{\rm min}$ is very significant. In (a) and (b), the Hub test finds very significant alignment for sources in regions where the S and Z tests also find very significant alignment. But only the Hub test finds the polarization directions in (c) aligned, so the Hub test and the S and Z tests do not always agree. In (d), one finds the map for the collection of sources from (a), (b), (c). That collection of sources is very significantly aligned. See Table 1 for some numerical details.

Ref. [7]. There, the regions dubbed 'RN1' and 'RN2' are centered at (RA,dec) = $(165°, 12°)$ and $(210°, 38°)$ extend over $(140° - 190°, 0° - 25°)$ and (RA,dec) = $(180° - 240°, 15° - 60°)$, whereas the regions in (a) and (b) of Fig. 4 have 24° radii centered on $(170°, 8°)$ and $(212°, 32°)$.

To test the agreement of the Hub test with the S and Z tests for Fig. 4 (a) and (b), we calculate the position angle PA for the direction from the centers of the regions in (a) and (b) to their respective hubs $H_{\rm min}$. We find that the PA for (a) is 138° and for (b) the PA is 57°. Both values fit nicely in the clump of PAs in Fig. 8 of Ref. [7]. The agreement confirms that the Hub test and the S and Z tests can yield similar conclusions about whether or not polarization directions align.

The sources of the region mapped in Fig. 4(c) lie midway between those of (a) and (b). Combining the sources in regions (a) and (b) with those in (c) gives the extended sample in (d). The total number of sources in (a), (b), (c) is 525, while the combination (d) has 365 sources, which implies that 160 sources straddle two regions. Comparing (c) and (d), one sees that the contour map in Fig. 4(d) is much like that in (c). By Table 1, the location of $\pm H_{\rm min}$ shifts only a couple of degrees from (c) to (d). Adding (a) and (b) to (c) makes little change. While (c) is the most significantly aligned region, the extended sample in (d) would rank eighth out of the 555 very significantly aligned regions. Of course, (d) is an extended region and not like the others, which are 24° radius regions.

| Fig. | Center (RA,dec) | $N$ | $\bar{\eta}_{\rm min}$ | $\pm H_{\rm min}$ (RA,dec) | Significance |
|---|---|---|---|---|---|
| 4(a) | $(170.^\circ, 8^\circ)$ | 140 | $37.3^\circ \pm 0.4^\circ$ | $(260.^\circ, -48^\circ) \pm (16^\circ, 3^\circ)$ | $5.9^{+4.8}_{-2.9} \times 10^{-3}$ |
| 4(b) | $(212^\circ, 32^\circ)$ | 204 | $37.8^\circ \pm 0.3^\circ$ | $(189^\circ, 16^\circ) \pm (8^\circ, 3^\circ)$ | $4.6^{+6.6}_{-2.9} \times 10^{-4}$ |
| 4(c) | $(190.^\circ, 20^\circ)$ | 181 | $36.4^\circ \pm 0.3^\circ$ | $(190^\circ, 0^\circ) \pm (1^\circ, 1^\circ)$ | $1.02^{+2.54}_{-0.76} \times 10^{-5}$ |
| 4(d) | Extended | 365 | $39.2^\circ \pm 0.4^\circ$ | $(188^\circ, 0^\circ) \pm (1^\circ, 1^\circ)$ | $4.8^{+10.8}_{-3.5} \times 10^{-5}$ |

Table 2: *The region center, number of sources, hub information, and significance for the samples in Fig. 4.* Uncertainties for $\bar{\eta}_{\rm min}$ and $\pm H_{\rm min}$ are found by fitting normal distributions to 200 runs using PPA $\psi$ distributed according to the $\sigma\psi$s listed in the JVAS/CLASS 8.4-GHz catalog. [6] The uncertainties in the Significance column are found by using the uncertainties in $c_i$ and $a_i$ from Table 1 in (16). Note that the center of the region (c) is just 1.3° from the average of the centers of (a) and (b), so the sources in (c) are midway between (a) and (b).

Since regions (c) and (d) trigger the Hub test, but not the S and Z tests, it follows that applying the Hub test can add useful information to the results obtained by the S and Z tests.

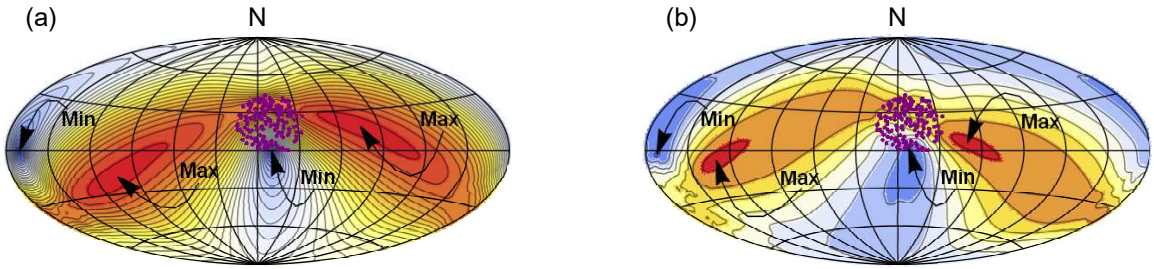


Figure 5: (Color online) *Simulations* These simulations have 181 sources located as in region Fig. 4(c), but the observed polarization directions are replaced with assigned values. (a) The polarization direction $\psi$ at each source is aligned perfectly with the hub $H_{\rm min}$ from Fig. 4(c). As a consequence, the minimum alignment angle vanishes, $\bar{\eta}(H_{\rm min}) = 0^\circ$. In (b), we simulate the observations in Fig. 4(c) by spreading out the polarization directions about the perfect alignment in (a). The observed polarization directions in Fig. 4(c) are consistent with the simulated result here for a $\delta\psi \approx \pm 50^\circ$ wide distribution about perfect alignment.

Two simulations are provided to illustrate these comments. The simulations have sources located as in Fig. 4(c) but the simulated sources are assigned new polarization directions that are not the measured directions.

The first simulation in Fig. 5(a) and Table 2(a) forces perfect alignment by aiming polarization directions directly toward the hub $H_{\rm min}$ that was obtained by observed data and mapped in Fig. 4(c). The contours near the targeted hub $H_{\rm min}$ make a tight bulls-eye pattern.

Comparing the perfect alignment map in Fig. 5(a) with the observed map 4(c) shows general similarities. Both have compact alignment near the hub $H_{\rm min}$ and wider regions of avoidance spread out around the hub $H_{\rm max}$. However, the alignment angle $\bar{\eta}$ for the targeted polarizations in 5(a) ranges over $\Delta\bar{\eta} = 65^\circ$ from $\bar{\eta}_{\rm min} = 0^\circ$ to $\bar{\eta}_{\rm max} = 65^\circ$. That compares with Fig. 4(c), where the range is much much less, with $\Delta\bar{\eta}$ only 16° from $\bar{\eta}_{\rm min} = 36^\circ$ to $\bar{\eta}_{\rm max} = 52^\circ$.

| Fig. | Center | $N$ | $\bar{\eta}_{\rm min}$ | $\pm H_{\rm min}$ | $\bar{\eta}_{\rm max}$ | $\pm H_{\rm max}$ | Significance of $\bar{\eta}_{\rm min}$ |
|---|---|---|---|---|---|---|---|
| 5(a) | $(189°, 20°)$ | 181 | $0°$ | $(190°, 0°)$ | $64.8°$ | $(256°, 18°)$ | 0 |
| 5(b) | $(189°, 20°)$ | 181 | $36.3°$ | $(188°, -2°)$ | $51.5°$ | $(230°, 6°)$ | $0.91^{+2.3}_{-0.69} \times 10^{-5}$ |

Table 3: *The region center, numbers of sources, hub information, and significance for the simulations in Fig. 5.* (a) Perfect alignment of the polarization directions with the hub $H_{\rm min}$ makes $\bar{\eta}_{\rm min}$ vanish by design. (b) Comparing the values here for Fig. 5(b) with those for Fig. 4(c) in Table 2, one concludes the observed map in Fig. 4(c) resembles perfect alignment in Fig. 5(a) except with polarization directions $\psi$ uncertain by $\delta\psi \approx 50°$, as in the simulation in Fig. 5(b).

To simulate the observed results in Fig. 4(c), let us degrade the perfect alignment in Fig. 5(a) by spreading out the polarizations directions. Thus, in (b), the assigned polarization directions are distributed normally about perfect alignment. Different choices give different maps. The selection displayed in Fig. 5(b) is chosen because the map looks like the one in Fig. 4(c). In the simulation Fig. 5(b), the half-width $\delta\psi$ of the PPA distributions is $\delta\psi = 48°$.

The map 5(b) matches 4(c), a conclusion that is reinforced by comparing the data listed in Tables 1 and 2 for 4(c) and 5(b). Thus, the observed polarization directions in region of Fig. 4(c) are consistent with an alignment of polarization directions toward the hub $H_{\rm min}$ with a normally distributed uncertainty of about $50°$.

# 5 Conclusions

The Hub test can help find and analyze large scale alignments of polarization vectors from sources such as QSOs. The test looks for correlations of polarization directions with directions toward points on the sphere. Similarly, correlations of polarization position angles PPA $\psi$ can be found with existing S and Z tests that compare polarization directions directly. However the results determined in the Hub test are distinct from and the implications differ from the results of the S and Z and similar tests.

Agreement can occur, for example, when polarization vectors aim in concert toward a Hub point that is far enough away from the sources, the polarizations collect around a common direction. In such cases, like that in Fig. 4(a), the S and Z tests as well as the Hub test detect alignment.

However, when polarization vectors aim in concert toward a Hub close to the sources, the behavior is not always detected by S- and Z-tests. Due to parallax, the polarization directions differ for sources located at different points on the sphere. Heuristically, directions can 'align' by pointing to the same hub. That provides an alternate meaning for the term 'aligned' and not the meaning assumed by the S and Z tests. Having both S and Z and like tests as well as the Hub test provides more insight into the nature of the alignments than either type of test can deliver on its own.

If the alignments found in Sec. 4 and in the references are not due to pure chance, then some mechanism needs to be found that explains them. The alignment of the samples in Fig. 4 occurs near the middle of the sources' distribution over the sky. Perhaps this could be evidence of a large scale electric current along the line of sight. By Ampere's Law, such a current seen end-on would produce a circulating magnetic field centered on the current's axis. By some process involving the medium between source and observer, the interaction with the intergalactic medium could reduce polarization parallel to the field. Radially-directed

polarizations would result. And that describes what is seen, polarizations directed toward a point near the middle of the affected region. Combining the Hub test with the S and Z tests may have uncovered a filamentary current in deep space or, perhaps, some other effect.

*Acknowledgments.* My thanks to V. Pelgrims for sending me the JVAS1450 catalog that gives redshifts and identifies the QSOs among the unclassified radio sources in the JVAS/CLASS 8.4-GHz catalog. Both V. Pelgrims and N. Ridge helpfully suggested including more content than appeared in earlier versions. This research did not receive any specific grant from funding agencies in the public, commercial, or not-for-profit sectors. Conflicts of interest: none.

# References

[1] D. Hutsemekers. Evidence for very large-scale coherent orientations of quasar polarization vectors. *Astronomy and Astrophysics*, 332:410–428, April 1998.

[2] P. Jain, G. Narain, and S. Sarala. Large-scale alignment of optical polarizations from distant QSOs using coordinate-invariant statistics. *MNRAS*, 347:394–402, January 2004.

[3] V. Pelgrims and J. R. Cudell. A new analysis of quasar polarization alignments. *MNRAS*, 442:1239–1248, August 2014.

[4] Damien Hutsemkers, Lorraine Braibant, Vincent Pelgrims, and Dominique Sluse. Alignment of quasar polarizations with large-scale structures. *Astron. Astrophys.*, 572:A18, 2014.

[5] Vincent Pelgrims and Damien Hutsemkers. Evidence for the alignment of quasar radio polarizations with large quasar group axes. *Astron. Astrophys.*, 590:A53, 2016.

[6] N. Jackson, R. A. Battye, I. W. A. Browne, S. Joshi, T. W. B. Muxlow, and P. N. Wilkinson. A survey of polarization in the JVAS/CLASS flat-spectrum radio source surveys - I. The data and catalogue production. *MNRAS*, 376:371–377, March 2007.

[7] V. Pelgrims and D. Hutsemékers. Polarization alignments of quasars from the JVAS/CLASS 8.4-GHz surveys. *MNRAS*, 450:4161–4173, July 2015.

[8] Emanuel Parzen. *Modern probability theory and its applications.* A Wiley publication in mathematical statistics. Wiley, New York, 1960.